5. Atmospheric CO_2 and $^{13}CO_2$ Exchange with the Terrestrial Biosphere and Oceans from 1978 to 2000: Observations and Carbon Cycle Implications

Charles D. Keeling, Stephen C. Piper,
Robert B. Bacastow, Martin Wahlen, Timothy P. Whorf,
Martin Heimann, and Harro A. Meijer

5.1 Introduction

Not only direct observations of CO_2 but also predictions from geophysical and biogeochemical models are needed to establish unequivocally the consequences of human activities on Earth's carbon cycle. During the industrial era, in which the combustion of fossil fuel contributed to a sharp rise in atmospheric CO_2 (Fig. 5.1), measurements of both the concentration and the $^{13}C/^{12}C$ ratio of atmospheric CO_2 are especially relevant. Our ability to predict correctly the time-varying gradients in atmospheric CO_2 that these data establish is an indispensable requirement for trusting models that link the storage of carbon in the atmospheric, terrestrial, and oceanic reservoirs of the carbon cycle to transfers of carbon between these global carbon pools.

These transfers, if thus validated, in turn can be compared with integrations of local flux measurements, carried out on land, for example by the AmeriFlux and EuroFlux eddy-correlation flux networks (Aubinet et al. 2000; Canadell et al. 2000) and in the oceans, for example by the joint Global Ocean Fluxes Study (Karl and Michaels 1996). Thus it is possible to combine top-down and bottom-up approaches to assess human impacts on the global carbon cycle.

To acquire an atmospheric CO_2 database adequate to establish human impacts on continental and global scales, it is necessary to sample air worldwide. This is most directly accomplished by collecting and analyzing flasks of atmospheric air or by continuous measurements of air at field sites (Keeling et al. 1989a).

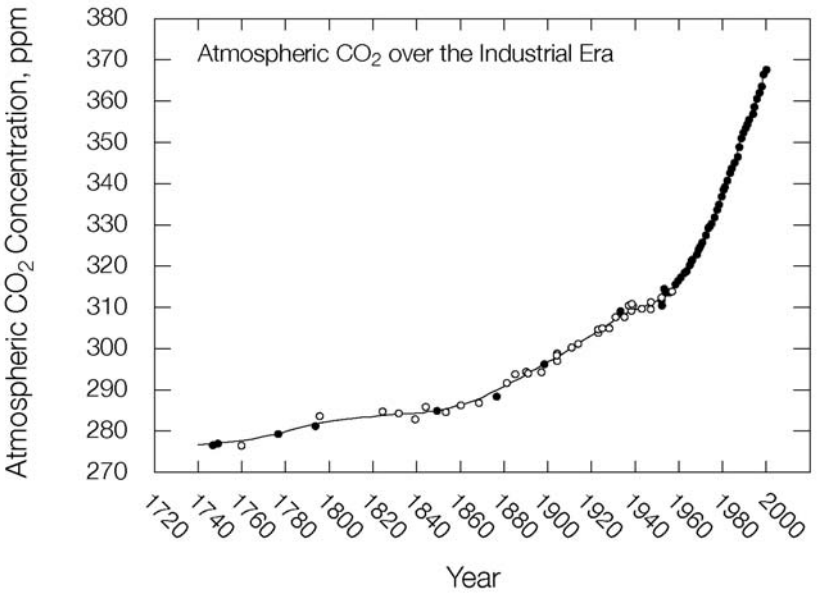

Figure 5.1. Time trend in the concentration of atmospheric CO_2, in ppm, from 1740 to 2000. Data before 1957 are proxies from measurements in air extracted from ice cores at Law Dome, Antarctica (open circles, Francey et al., 1995; closed circles, Etheridge et al., 1996). Data from 1957 to 1978 are averages of measurements from the South Pole and Mauna Loa Observatory. Data from 1978 on are averages of direct measurements of air collected from 6 to 9 locations (closed circles). The curve is a spline function that combines separate fits to the proxy and direct data as described by Keeling et al. (1989a).

Because atmospheric turbulence tends to smooth out the effects of local sources and sinks on the atmospheric CO_2 distribution, only a limited number of sampling locations are required. They must, however, be remote from large local sources and sinks of CO_2. In this chapter we interpret atmospheric CO_2 data, updating an earlier study (Keeling et al. 1989a). This new study again depends on data from fewer stations than do most other recent global studies, but that lack is offset to a considerable degree because it uses a more extensive isotopic data set.

The study has two approaches: first, as reported provisionally by Keeling et al. (2001), to calculate and interpret global average exchanges of atmospheric CO_2 with the terrestrial and oceanic carbon reservoirs that together sum to all globally significant exchanges; second, as reported provisionally by Piper et al. (2001), to calculate a set of regional "source components" that together sum to all globally significant exchanges.

Here we describe results mainly on the global approach. The source components, which also apply to the global scale study, include industrial emissions

of CO_2. These components include industrial emissions of CO_2 and long-term human-induced disturbances to terrestrial vegetation and of soils; also included are the perturbations induced by these disturbances, such as the uptake of CO_2 by the oceans and terrestrial vegetation, and the natural CO_2 fluxes. In constructing these components, which portray both sources and sinks of atmospheric CO_2, we make use of *a priori* information as much as possible, including global data sets, on a spatial grid, of observed sea and land surface temperatures and of terrestrial photosynthetic activity derived from remote sensing data observed by satellites.

For the less reliably known components, we prescribe, *a priori,* only their spatial and temporal structures, adjusting their overall strengths simultaneously to predict optimally our observations of CO_2 concentration and $^{13}C/^{12}C$, taking account of the entire set of component fluxes. Here, we compute only global average exchanges of atmospheric CO_2. These exchanges, which transfer CO_2 to and from terrestrial vegetation and soils (henceforth, together called the "terrestrial biosphere") and to and from the world oceans (henceforth, "oceans"), are inferred from global averages of time-varying concentration and $^{13}C/^{12}C$ ratio determined from our observations.

A major challenge is to determine how time-varying sources and sinks of atmospheric CO_2 reflect the interplay of natural processes and human activities, including feedbacks between Earth's carbon cycle and its physical environment. Of paramount interest is that Earth's heat balance is being altered by an enhanced greenhouse effect caused by rising concentrations of CO_2 and other infrared-absorbing gases. Global warming is likely to be occurring as a consequence, altering the carbon cycle globally (Santer et al. 1996; Crowley 2000). The picture is complicated, however, because natural variations in climate also impact Earth's heat balance (Free and Robock 1999; Andronova and Schlesinger 2000) and the carbon cycle (Falkowski et al. 2000).

Although the observations most essential to this study are measurements of CO_2 concentration, valuable information is afforded by its $^{13}C/^{12}C$ ratio, expressed in delta notation as

$$\delta^{13}C = (R_{sample} - R_{standard})/R_{standard} \tag{5.1}$$

where R denotes the measured $^{13}C/^{12}C$ molar ratio of a specific sample of CO_2, and the subscripts refer to the measured sample and the international standard (PDB). Because the rare stable isotope (^{13}C) is strongly fractionated during photosynthesis by land plants, the terrestrial biosphere alters the $\delta^{13}C$ of atmospheric CO_2 far more than do the oceans (Farquhar, Ehleringer, and Hubick 1989; Keeling et al. 1989a). Terrestrial and oceanic CO_2 fluxes can thus be distinguished using $\delta^{13}C$ data, with certain additional information, including variability in the fractionation factor for photosynthesis for different types of plants and under different growing conditions and, on long timescales, evidence of the degree of vertical mixing of the oceans.

5.2 Atmospheric Observations

Observations of atmospheric CO_2 concentration and its $^{13}C/^{12}C$ ratio, expressed by $\delta^{13}C$, were obtained from an array of 10 stations situated along a nearly north-south transect mainly in the Pacific Ocean basin. The stations extend from the Arctic to the South Pole (Fig. 5.2), at sites on land located as far as possible from biological activity and combustion of fossil fuels.

By sampling the air upwind, we minimized the effects of local interferences, so the observations mainly reflect broadscale CO_2 fluxes. The concentration data set begins in 1957, the isotopic data set in 1977. The data provide complete time-series for all stations of the array from 1986 onward. Here we mainly consider data after 1977. The CO_2 concentration C is expressed as a mole fraction in parts per million of dry air (ppm), the isotopic data, $\delta^{13}C$, in per mil (‰) departures from the standard PDB (Craig 1957; Mook and Grootes 1973). Methods of sampling, measurements, and calibrations are described in Keeling et al. (2001).

The CO_2 concentration decreases almost monotonically from north to south such that two Arctic stations, Alert and Point Barrow, register concentrations 3 to 5 ppm higher than the most southerly stations, in New Zealand and at the South Pole (Fig. 5.3A, Alert not shown).

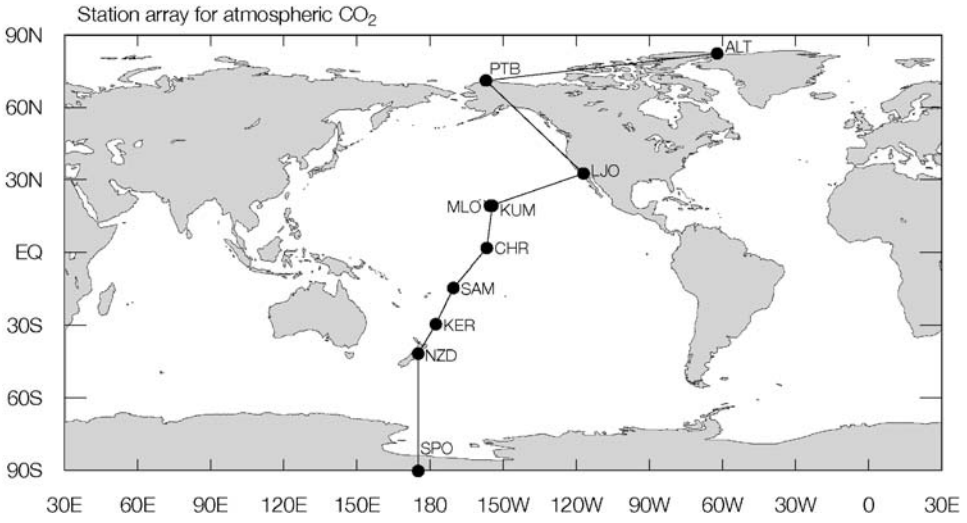

Figure 5.2. Locations of carbon dioxide sampling stations that furnish data for Keeling et al. (2001). Station symbols: ALT = Alert; PTB = Point Barrow; LJO = La Jolla; KUM = Cape Kumukahi; MLO = Mauna Loa Observatory; CHR = Christmas Island; SAM = Samoa; KER = Kermadec; NZD = New Zealand; SPO = South Pole. Further information is listed in Table 5.1. A transect connecting the stations is shown.

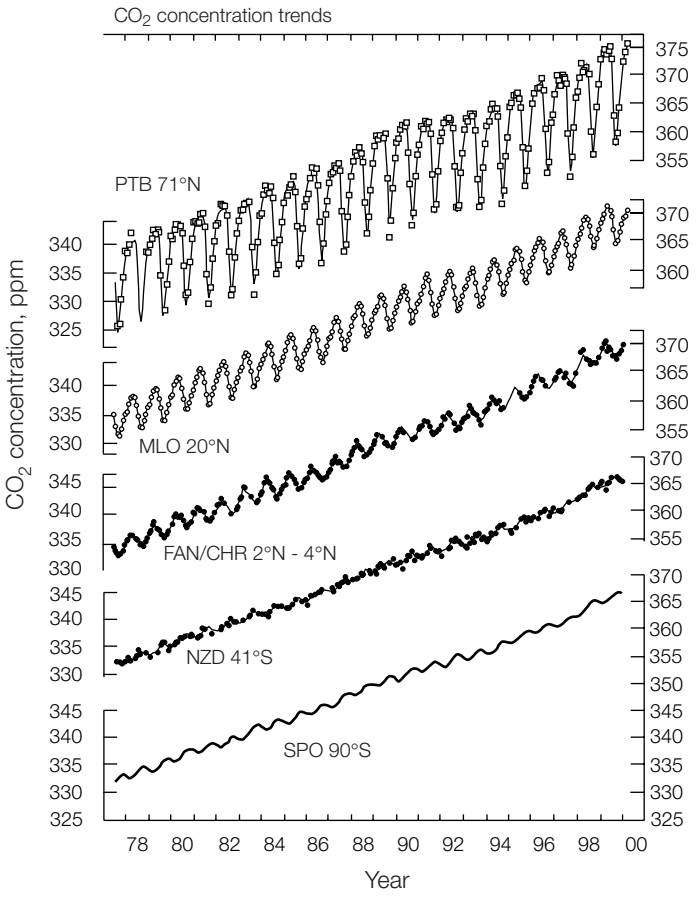

Figure 5.3. Trends in the measured atmospheric CO_2 concentration and its carbon isotope ratio, $\delta^{13}C$. **(A)** Concentration, in ppm, in the Northern and Southern Hemispheres, respectively, shown by monthly averages (dots) and by a smooth curve consisting of the sum of four seasonal harmonics and a spline function (solid lines). The seasonal harmonics include a linear gain factor, to represent increasing amplitude with time. **(B)** Same, respectively, for carbon isotope ratio, $\delta^{13}C$, in ‰. Station code names are as defined in Fig. 5.2. FAN/CHR refers to data for Fanning and Christmas Islands, combined. The scale of $\delta^{13}C$ is inverted so that seasonal patterns of concentration and $\delta^{13}C$ appear with the same phasing. Data are from Keeling et al. (2001).

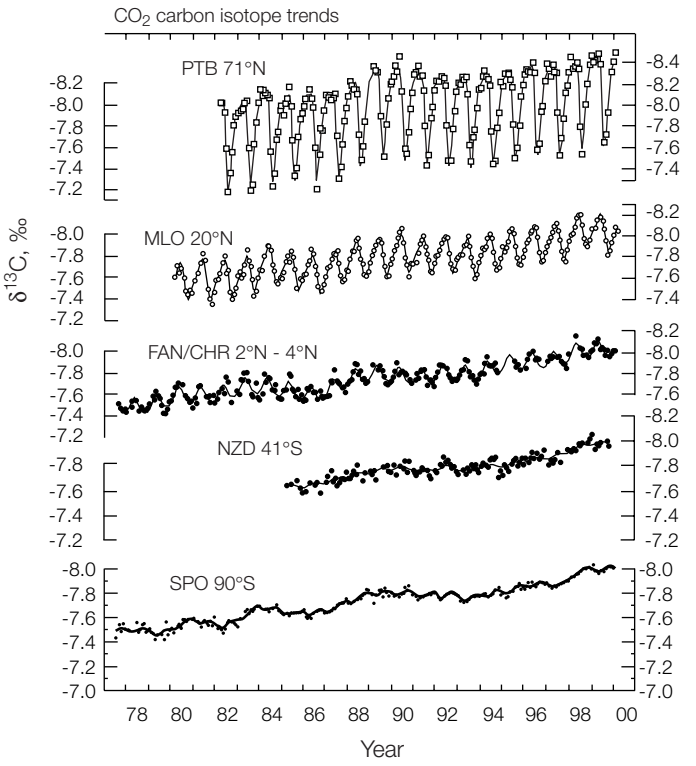

Figure 5.3. *Continued.*

The main cause of the southward decrease is the predominance of industrial emissions of CO_2 in the Northern Hemisphere (Keeling, Piper, and Heimann 1989b). These emissions, in addition, have caused $\delta^{13}C$ of atmospheric CO_2 (Fig. 5.3B) to increase from north to south, because fossil fuels are strongly depleted in the heavy carbon isotope relative to atmospheric CO_2, a reflection of their origins as plant carbon. The explanation for the north-south isotopic gradient in CO_2 is more complicated, however, owing to isotopic fractionation processes not associated with photosynthesis of land plants. Of these processes, the most important is temperature-dependent isotopic fractionation in the air-sea exchange of CO_2 which promotes negative $\delta^{13}C$ at high latitudes relative to low latitudes, and in the Southern Hemisphere relative to the Northern (Keeling et al. 1989a).

Short-term interannual variations in concentration and $\delta^{13}C$ exhibit similar temporal patterns at individual stations and, to a considerable extent, similar patterns from station to station. Emissions of industrial CO_2, because they vary only slightly from year to year, contribute little to these temporal patterns. There-

fore, because the $\delta^{13}C$ variations are relatively large, the similarities seen in the patterns imply that terrestrial biospheric fluxes are the dominant cause of short-term variations in CO_2 concentration, as well as in $\delta^{13}C$.

We identified quasi-periodic variability in atmospheric CO_2 distinguished by time-intervals during which the seasonally adjusted CO_2 concentration at Mauna Loa Observatory, Hawaii, rose either more rapidly or less rapidly than a long-term trend line proportional to industrial CO_2 emissions. The Mauna Loa data and the trend line are shown in Fig. 5.4 with vertical gray bars demarking the intervals of rapidly rising CO_2.

Data from Mauna Loa Observatory were chosen for this identification because the measurements there are continuous and thus provide a more precisely determined rate of change than could any other station in our observing program. An association of rapidly rising CO_2 with temperature is seen consistently in the Mauna Loa record since it began, in 1958 (Keeling et al., 1989a; Keeling et al., 1995). As first noted by Bacastow (1976), rapidly rising CO_2 concentrations typically occur during El Niño events, involving almost global scale changes in temperature and identifiable by low Southern Oscillation Index (SOI) values (Rasmusson and Wallace 1983; Meehl 1987). The SOI indeed shows low values at times of some of the gray bars, but not all (see Fig. 5.4).

The SOI tracks the surface barometric pressure difference across the Pacific Ocean in the tropics. This pressure difference weakens during El Niño events and strengthens during the opposite phase in a so-called El Niño–Southern oscillation (ENSO) cycle. On three occasions during the time-period (1983, 1987, and 1998), there were pronounced minima in the SOI followed by sharp increases. Very strong El Niño events occurred at these times, accompanied by both strong warming and prominent increases in the rate of the rise of atmospheric CO_2 (Slingo and Annamalai 2000). The timing of an SOI minimum for these events almost exactly coincides with the commencement of a gray bar, and this suggests a remarkably close phase relation to the rate of atmospheric CO_2 rise. The SOI-CO_2 relation during a prolonged period of low SOI values from 1992 through 1994 is less consistent, indeed, the least consistent for the entire 42 years of the Mauna Loa record. A sharp decrease in rate of rise of CO_2 began immediately after the volcanic eruption of Mt. Pinatubo in 1991 and persisted until 1993. Then CO_2 began to rise in evident association with the dissipation of a volcanic dust veil that had promoted cool temperatures after the eruption (Keeling et al. 2001). The commencement of a gray bar in late 1993 is evidently not related to the ENSO cycle, although the long duration of the gray bar interval probably marks a return to the SOI-CO_2 association seen in the three prominent events already noted. The gray bars near 1980 and 1990 are associated with global warming, not evidently correlated with El Niño events. Also, there is no gray bar at the time of a weak El Niño event in 1992, probably because this event was during the period of cooling associated with the Pinatubo eruption. Thus the gray bars shown in Fig. 5.4 identify times of the ENSO cycle of the past 22 years when it involved strong oscillations in the

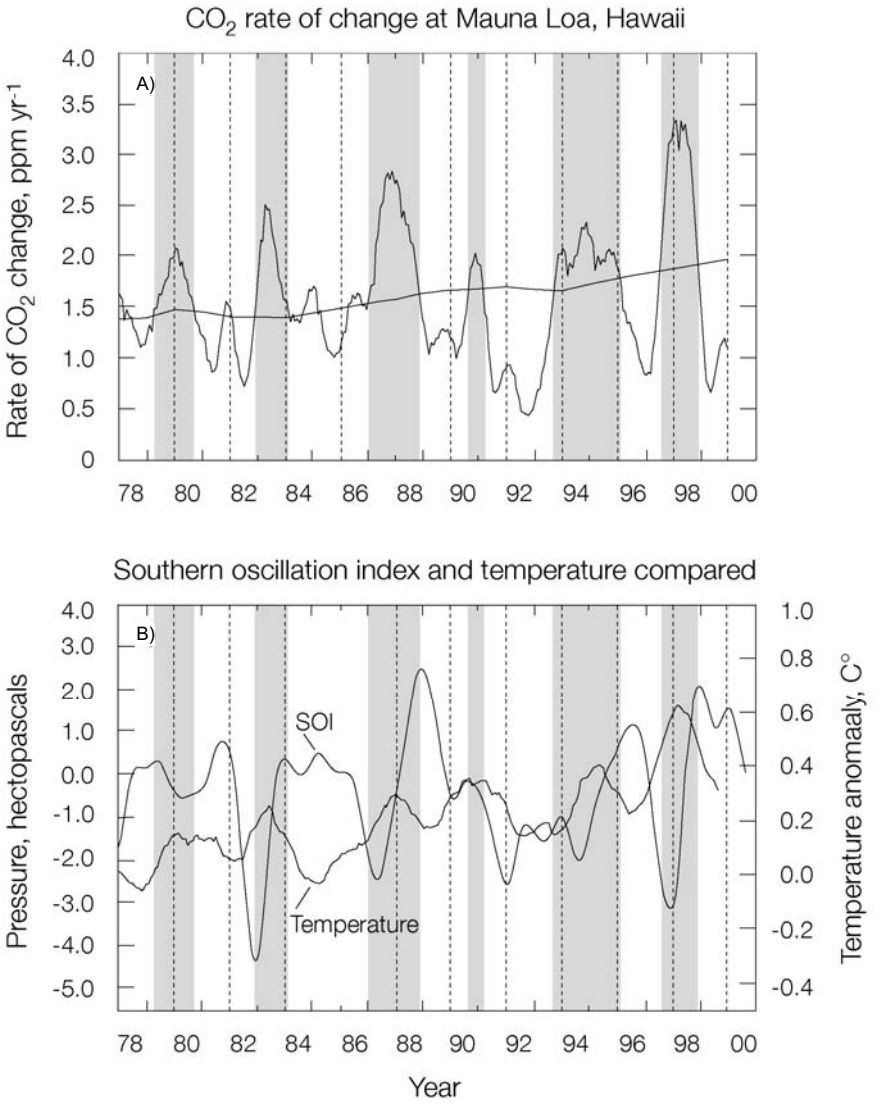

Figure 5.4. Comparison of quantities that vary with the El Niño–Southern Oscillation (ENSO) Cycle. **(A)** Rate of change of atmospheric CO_2 concentration, in ppm yr^{-1}, at Mauna Loa Observatory, Hawaii (strongly fluctuating curve), plotted together with the industrial CO_2 release (slowly rising curve). The latter trend is defined as the average fraction of emissions of industrial CO_2 that remained airborne as determined by Keeling et al. (1995) to be 58.1%. **(B)** The Southern Oscillation Index (SOI, thin line), determined as the barometric pressure difference of Tahiti minus Darwin, Australia, in hPa, and global average temperature anomaly (thicker line). The SOI data were derived from Climate Prediction Center (2000), the temperature data from Jones (1994, and personal communication). Vertical gray bars in both panels indicate timeintervals during which the rate of change of atmospheric CO_2 at Mauna Loa exceeded the industrial CO_2 trend rate.

SOI and was not complicated by a very powerful volcanic eruption; they also, however, identify times of rapid warming not clearly associated with the ENSO cycle.

We estimated the global average concentration and carbon isotope ratio of atmospheric CO_2 from 1978 through 1999 (Keeling et al. 2001, Appendix D). The resulting time-series are shown in Fig. 5.5.

For modeling purposes, these time-series were extended back to A.D. 1740. The extension of the CO_2 concentration series (see Fig. 5.1) consists of data from air trapped in glacial ice collected at Law Dome, Antarctica, assumed to represent the global average concentration, and after 1955 from direct observations. The extension of the $\delta^{13}C$ series was created by a deconvolution procedure, making use of the global CO_2 concentration time-series to establish chemical disequilibria of the global carbon cycle, assuming that the atmospheric, terrestrial biospheric, and oceanic carbon reservoirs were at chemical and isotopic equilibria in 1740. The $^{13}C/^{12}C$ ratio in 1740 was set so that the $\delta^{13}C$ value in 1978 exactly agreed with observations.

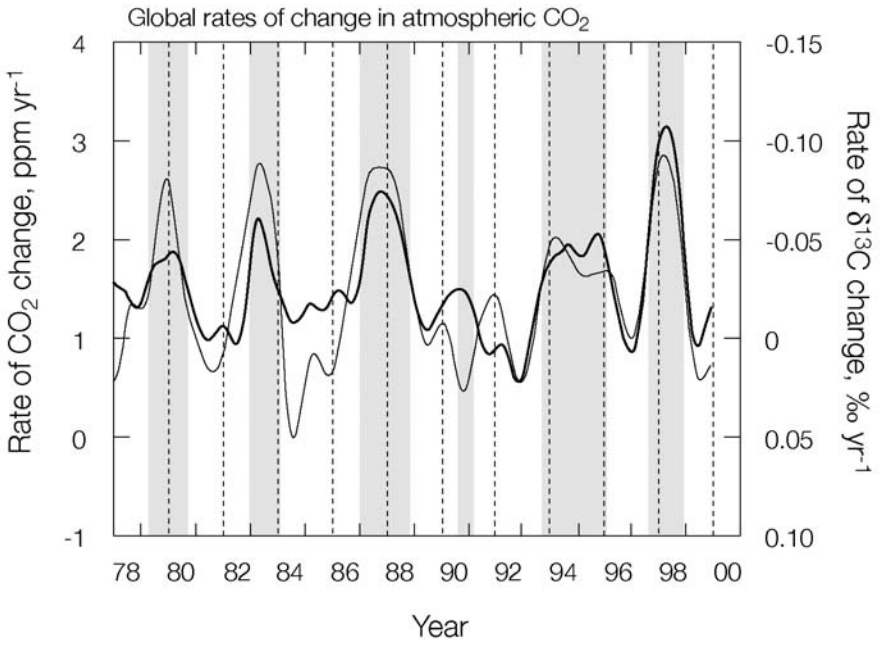

Figure 5.5. Rates of change of globally averaged atmospheric CO_2 concentration, in ppm (thick line), and $\delta^{13}C$, in ‰ (thin line), computed from the time-trends shown in Keeling et al. (2001). Gray bars are as in Fig. 5.4.

5.3 Isotopic Signature of the Seasonal CO_2 Cycle

The concentration of atmospheric CO_2 and its reduced carbon isotope ratio (see Fig. 5.3) covary over their seasonal cycles, because the $\delta^{13}C$ value of the carbon of land plants is distinctly more negative than that of atmospheric CO_2, and the seasonality of plant growth and respiration are the dominant causes of seasonality in atmospheric CO_2. Over the Northern Hemisphere, where this seasonality is a prominent feature of the CO_2 records, the $\delta^{13}C$ values inferred to be exchanged between the terrestrial biosphere and the atmosphere over each annual cycle tend to approach that of CO_2 respired by land plants (Mook et al. 1983; Heimann, Keeling, and Tucker 1989; Pataki et al. 2003). In the Southern Hemisphere, however, plant activity produces only small seasonal cycles in CO_2 concentration and $\delta^{13}C$; consequently, the average $\delta^{13}C$ value that explains the covariance of the seasonal cycle in that hemisphere is not precisely established (Keeling et al. 2001).

In our atmospheric records in the Northern Hemisphere, slight trends can be discerned toward more negative $\delta^{13}C$ values inferred from CO_2 fluxes from decade to decade, in addition to short-term interannual variability (Keeling et al. 2001). The decadal trends do not significantly differ from the average $\delta^{13}C$ trend of atmospheric CO_2, shown on each plot by a straight line. The carbon isotope discrimination term ($^{13}\Delta_{cov}$) that explains the seasonal covariance of $\delta^{13}C$ and CO_2 concentration is

$$^{13}\Delta_{cov} = \delta^{13}C_I - \delta^{13}C_0 \tag{5.2}$$

where the subscript I refers to CO_2 attributed to plant metabolism combined with oceanic CO_2 exchange, and subscript o refers to background atmospheric CO_2. The Arctic stations and La Jolla show little interannual variability in $\delta^{13}C_I$; Mauna Loa and Cape Kumukahi show possibly significant annual variations in the range of 2‰. For these northern stations, where oceanic CO_2 exchange has only a small or a negligible effect on the seasonal cycle of atmospheric CO_2, $^{13}\Delta_{cov}$ is close to the isotopic discrimination for photosynthesis of land plants, suggesting that this discrimination, averaged over large regions, has varied temporally by 1 to 2‰ during the past decade. With respect to latitude, averages of $\delta^{13}C_I$ from 1992 to 1999 show little evidence of variation within either hemisphere, but the hemispheric averages differ sharply: −27.5‰ in the Northern, −17.5‰ in the Southern (Keeling et al. 2001). The lower average for $\delta^{13}C_I$ in the Southern Hemisphere is consistent with a significant contribution to the seasonal cycle of atmospheric CO_2 by oceanic exchange, with its far lower isotopic discrimination than terrestrial exchange. To an indeterminate extent, the lower average may also reflect that a greater part of the vegetation on land in the Southern Hemisphere uses a photosynthetic pathway, C_4, with much lower fractionation than that of the more common C_3 pathway.

5.4 Deconvolution of Global Data

To resolve globally averaged temporal variations in atmospheric CO_2 into terrestrial and oceanic components, we employ an inverse procedure. First, by what we call a "single deconvolution," we deduce the oceanic and terrestrial CO_2 exchange fluxes solely from atmospheric CO_2 concentration data. Then, by a "double deconvolution," we adjust these estimates to be consistent with the $\delta^{13}C$ value of atmospheric CO_2.

In these calculations we identify only the most significant global pools of carbon affecting contemporary atmospheric CO_2: an oceanic pool consisting mainly of bicarbonate and carbonate salts; a terrestrial biospheric pool consisting of organic carbon stored in living plants, detritus, and soils; and a fossil fuel pool representing the available resource of coal, petroleum, and natural gas, combined. The associated global average exchange fluxes of CO_2 we denote as F_{oce}, F_{bio}, and F_{ind}, respectively. The industrial flux (F_{ind}) includes a small contribution from the manufacture of cement (Andres et al., 2000), while F_{oce} and F_{bio} represent net fluxes that are the relatively small differences between large one-way fluxes. All fluxes will be expressed here in petagrams of carbon (Pg C $= 10^{12}$ kg of carbon). To a close approximation, the sum of the three time-dependent fluxes determine the rate of change of atmospheric CO_2 abundance, N_a, expressed by the mass-conserving global atmospheric carbon cycle budget equation

$$dN_a/dt = F_{ind} + F_{oce} + F_{bio} \tag{5.3}$$

Over the past two decades the average strengths of the terms of Equation 5.3 are approximately as follows: The concentration of atmospheric CO_2 has risen at about 3.5 Pg C yr^{-1}, a little over half the rate of industrial emissions, which are about 6 Pg C yr^{-1} (see Chapter 18). The atmospheric CO_2 budget is balanced by an oceanic sink of about 2 Pg C yr^{-1} and by a terrestrial sink of about 0.5 Pg C yr^{-1}.

To specify this budget in greater detail, we distinguish several different contributions to the net exchange fluxes involving the oceanic and terrestrial biospheric carbon pools (Keeling et al., 1989a). We divide the net oceanic exchange flux into two components

$$F_{oce} = F_{ex} + F_{ano,oce} \tag{5.4}$$

where F_{ex} denotes the expected oceanic response to rising atmospheric CO_2 concentrations, and $F_{ano,oce}$ an "anomalous" flux representing a remainder not captured by F_{ex}. We divide the net terrestrial biospheric exchange flux into three components

$$F_{bio} = F_{fer} + F_{des} + F_{ano,bio} \tag{5.5}$$

where F_{fer} represents plant growth stimulated ("fertilized") by elevated atmospheric CO_2 concentration relative to the concentration in 1740, and F_{des} represents the release of CO_2 from the terrestrial biosphere owing to biologically destructive human-caused land-use changes, including deforestation and biomass burning. An "anomalous" flux, $F_{ano,bio}$, denotes a remainder not explained by either of the previously identified processes. In the procedure for single deconvolution, which we begin with atmospheric CO_2 concentration data for 1740 (Keeling et al., 1989a, 2001), we compute the expected oceanic response, F_{ex}, to rising atmospheric CO_2 concentration, using the one-dimensional vertically resolved oceanic box-diffusion model of Siegenthaler and Oeschger (1987). This oceanic submodel is characterized by a vertical diffusion coefficient, K, and an air-sea CO_2 exchange coefficient, k_{am}; it yields an oceanic sink as a function of atmospheric CO_2 concentration that agrees quite closely with estimates from three-dimensional oceanic circulation models (Keeling et al. 1989a). We do not regard its temporal variability as a reliable estimate of the true short-term interannual variability in F_{oce}. A substantial portion of that variability is found to reside in the anomalous oceanic flux, $F_{ano,oce}$, established later, in the double deconvolution calculation.

In the single deconvolution, we also compute the expected terrestrial biospheric response, F_{fer}, to rising atmospheric CO_2, using a terrestrial submodel controlled by a "growth factor." This factor, denoted β_a by Keeling et al. (1989a), expresses the degree to which the increase in atmospheric CO_2 concentration after 1740 caused enhanced plant uptake of CO_2, expressed as a linear growth response of plants to increasing CO_2 concentration resulting from a stimulation of net primary production (NPP) (Keeling et al. 1989a). For β_a, we have adopted the value 0.41, signifying that the increase in uptake by long-lived biospheric carbon has been 41% of the fractional increase in CO_2 concentration, where the NPP of long-lived carbon in 1740 was calculated to be 24.6 Pg C yr^{-1}. (The deconvolution calculations would yield almost the same outputs if, by the inclusion of short-lived biospheric carbon, β_a had been assigned a value of 0.18 with respect to total NPP, the latter calculated to be about 56 Pg C yr^{-1} for 1982 (Heimann and Keeling 1989). The destructive land-use flux, F_{des}, and the anomalous flux, $F_{ano,\,bio}$, are not determined in this calculation.

The calculations of the single deconvolution are repeated via an iterative scheme that adjusts $F_{ano,oce}$ and the sum $F_{ano,bio} + F_{des}$ at each step so that both the $\delta^{13}C$ values and concentration of atmospheric CO_2 agree with observations. This double deconvolution procedure reconciles the global atmospheric CO_2 budget, expressed by Equation 5.3 for the sum of the two isotopes, ^{13}C and ^{12}C, and a similar budget equation for the rare isotope, ^{13}C, alone.

The terrestrial biospheric exchange flux, F_{bio}, of Equation 5.3 represents the difference between two large one-way CO_2 fluxes. These we denote by F_{ab}, an atmospheric CO_2 sink owing to assimilation of CO_2 by plants through photosynthesis, and F_{ba}, an atmospheric CO_2 source owing to respiratory processes involving decay of vegetative matter. Thus,

$$F_{bio} = F_{ba} - F_{ab} \tag{5.6}$$

Both one-way fluxes apply to carbon in general, and thus to the isotopic sum, $^{13}C + {}^{12}C$. Correspondingly, for ^{13}C the net flux is

$$*F_{bio} = *F_{ba} - *F_{ab} \tag{5.7}$$

where the asterisks denote fluxes of ^{13}C alone. The one-way ^{13}C fluxes are related, respectively, to the one-way fluxes for $^{13}C + {}^{12}C$ by the expressions

$$*F_{ab} = \alpha'_{ab} R_a F_{ab} \tag{5.8}$$

$$*F_{ba} = \alpha'_{ba} R_b F_{ba} \tag{5.9}$$

where R_a and R_b denote, respectively, the ratios $^{13}C/(^{13}C + {}^{12}C)$ of atmospheric CO_2 and of carbon in the terrestrial biospheric pool, and α'_{ab} and α'_{ba} denote fixed $^{13}C/(^{13}C + {}^{12}C)$ isotopic fractionation (discrimination) factors. Corresponding factors with respect to $\delta^{13}C$ values are denoted below by α without the prime sign.

We set α_{ab}, which represents an isotopic discrimination of 15.32‰ against ^{13}C associated with photosynthesis (see below), to 0.98468 (i.e., to 1–15.32/1000), and we set α_{ba}, equal to unity, by assuming, consistent with earlier calculations (Keeling et al., 1989a), that no isotopic fractionation accompanies respiration. We then compute their α' equivalents, making use of the relationship (Heimann and Keeling 1989)

$$R_i = r_i(R_s/r_s) \tag{5.10}$$

where R_s and r_s denote, respectively, the $^{13}C/(^{13}C + {}^{12}C)$ and $^{13}C/^{12}C$ ratios of the international standard PDB, and the subscript i refers to any given carbon pool. Equations 5.8 and 5.9 are then rewritten

$$*F_{ab} = \alpha'_{ab} r_a (R_s/r_s) F_{ab} \tag{5.11}$$

$$*F_{ba} = r_b (R_s/r_s) F_{ba} \tag{5.12}$$

where r_a and r_b denote $^{13}C/^{12}C$ ratios corresponding respectively to R_a and R_b. Similar expressions apply to CO_2 exchange with the oceans, as follows:

$$F_{oce} = F_{ma} - F_{am} \tag{5.13}$$

$$*F_{am} = \alpha'_{am} r_a (R_s/r_s) F_{am} \tag{5.14}$$

$$*F_{ma} = \alpha'_{am} <\alpha'_{eq}> r_m (R_s/r_s) F_{ma} \tag{5.15}$$

where F_{ma} denotes the one-way gross flux of CO_2 from the well-mixed surface layer of the oceans to the atmosphere, F_{am} the reverse flux, and R_m and r_m, respectively, the ^{13}C ($^{13}C + {}^{12}C$) and $^{13}C/^{12}C$ ratios of the well mixed surface layer of the ocean. The symbol $<\alpha'_{eq}>$, equal to $\overline{\alpha'_{ma}/\alpha'_{am}}$, denotes the global annual average $^{13}C/(^{13}C + {}^{12}C)$ equilibrium fractionation factor for air-sea exchange of CO_2. For convenience, we next express most of the results of our double deconvolution calculations as reduced isotope ratios, defined by Equation 5.1, where δ_a, δ_b, and δ_m denote δ^{13} C of atmospheric CO_2, terrestrial carbon, and carbon in surface seawater, respectively. Also, we express isotopic fractionation between carbon pools by fractionation terms with respect to $^{13}C/^{12}C$ ratios by the expression

$$\varepsilon_{ij} = \alpha_{ij} - 1 \tag{5.16}$$

where i and j denote, respectively, donor and receiver pools.

In most of the calculations, the $^{13}C/^{12}C$ fractionation factor, α_{ab} (equivalently expressed by ε_{ab}), is assumed to be constant (Keeling et al. 1989a). However, below we will discuss the consequences if this factor, which represents the isotopic discrimination of plants during photosynthesis, is allowed to vary. The factor α_{am}, which represents fractionation attending oceanic uptake, is assumed to be constant. The associated factor α_{ma}, however, is assumed to vary with sea surface temperature, and hence with time, because the equilibrium fractionation, α_{eq} (equal to the quotient α_{ma}/α_{am}), is temperature dependent, as discussed below.

The $^{13}C/^{12}C$ isotopic ratio for F_{fer} expressed by annual averages, is set equal to $\alpha_{ab}r_a$, the same ratio as that of CO_2 assimilated by plants during photosynthesis (Heimann and Keeling 1989). The $^{13}C/^{12}C$ ratio associated with the sum, $F_{des} + F_{ano,bio}$, is set equal to r_b, computed by taking account of the average storage time of long-lived carbon in the terrestrial pool (Keeling et al. 1989a).

The magnitude of the global average $^{13}C/^{12}C$ fractionation factor for CO_2 assimilation during plant growth, α_{ab}, affects the computed values of $\delta^{13}C$ for all of the biospheric fluxes in the deconvolution calculations (see Heimann and Keeling 1989). The value that we assign to α_{ab} depends on the relative contributions from C_3 and C_4 plants. These pathways have distinctly different degrees of discrimination against ^{13}C, which may vary with time; in addition, the relative contribution of the two plant types may vary with time. These possible temporal variations are disregarded in our double deconvolution calculations.

The single deconvolution predicts monthly values of all of the exchange CO_2 fluxes defined above and the amounts and $^{13}C/^{12}C$ ratios of carbon in the atmospheric, oceanic, and terrestrial carbon pools. The $^{13}C/^{12}C$ ratios for atmospheric CO_2, so obtained, are then used in initializing the double deconvolution calculation in 1978 by setting the value in 1740 such that the predicted annual value agrees with our isotopic observations in 1978.

The destructive land-use flux, F_{des}, always positive, is computed only for the

time-period of the double deconvolution; it is set equal to 2.0 Pg C yr^{-1}, the average for 1980–1989 as given by Houghton (1999). The term, $F_{ano,bio}$, is then calculated by difference to be consistent with Equation 5.5. The relative contributions of F_{fer}, F_{des}, and $F_{ano,bio}$ to the overall net biospheric flux, F_{bio}, though uncertain, only slightly affect the computations of the double deconvolution, because the $^{13}C/^{12}C$ ratios for the three fluxes are nearly the same.

5.5 Isotopic Discrimination by Terrestrial Vegetation

The C_3 photosynthetic pathway of terrestrial plants produces an isotopic discrimination with a typical value of about 18‰ relative to the $^{13}C/^{12}C$ ratio of atmospheric CO_2, and a range for different species of several per mil (Farquhar et al. 1989). Although C_3 plants account for most of net primary production (NPP), plants with the C_4 pathway contribute about 20‰ of global NPP with a discrimination of only about 4‰ (Farquhar al. 1989; Still et al. 2003). Consequently, the global average fractionation factor, α_{ab}, defined earlier, is less than for C_3 plants alone.

To estimate α_{ab}, we adopted a carbon isotope discrimination for C_3 plants of 17.8‰, and for C_4 plants of 3.6‰, as reported by Lloyd and Farquhar (1994). We then computed NPP for C_3 and C_4 plants for selected geographic zones using a vegetation map (Hunt et al. 1996) that prescribes types of biomes at a resolution of 1 degree. For each grid point of the map, NPP was computed by a method that makes use of remotely sensed radiometric data, from 1982–1990, the only period for which reliable radiometric data were available. The resulting global average fraction of NPP contributed by C_4 plants is found to be 17.44‰, leading to a global average discrimination for C_3 and C_4 plants combined of 15.32‰. This calculation of global average carbon isotope discrimination does not take into account subzonal-scale or temporal variability in discrimination of the separate plant types, C_3 and C_4, issues that we discuss next.

For the Northern Hemisphere, discrimination varies in the range from 17.8‰ at high latitudes, to 14.0‰ in the tropics, as the C_4 fraction of NPP varies from 0 to 27%. For the two extratropical zones, where NPP is mainly owing to C_3 plants, discrimination is 1.8‰ less than that inferred from the covariance of atmospheric CO_2 concentration and isotope ratio, $^{13}\Delta_{cov}$, observed for stations in the Northern Hemisphere.

In the tropics and farther south, the likelihood of substantial oceanic influence on $^{13}\Delta_{cov}$ precludes obtaining reliable estimates of plant discrimination from our station data. It is probably reasonable to assume that the discrimination of C_3 plants south of the tropics is nearly the same as north of the tropics, and that the effect of discrimination of C_4 plants is too small for our neglect of its zonal variability to influence our calculations.

Temporal variability in discrimination of C_3 plants is more likely to be a serious neglect in our computations than spatial variability. Such variability is expected because the degree of isotopic discrimination varies with stomatal con-

ductance of plant leaves. When stressed by lack of adequate water, plant stomata tend to close, reducing the carbon isotopic fractionation that can occur at the primary sites of CO_2 fixation within the leaves (Farquhar et al. 1989; Ehleringer, Hall, and Farquhar 1993). Ometto et al. (2002) and Fessenden and Ehleringer (2003) have presented evidence of interannual variability in C_3 plant discrimination. Since variable water stress affects much of the world's vegetation, a global average temporal variation of 2‰ or more seems likely based on these studies.

To examine how variable discrimination against the rare isotope, ^{13}C, by land plants may affect the net biospheric exchange flux, F_{bio}, as calculated in our double deconvolution procedure, we invoke isotopic additivity to establish the shift in $\delta^{13}C$ of atmospheric CO_2 that takes place when atmospheric CO_2 is exchanged with the terrestrial biosphere:

$$(\delta^{13}C)\mu = (\delta^{13}C_o)\mu_o + \delta^{13}C_I(\mu - \mu_o) \tag{5.17}$$

where μ denotes the atmospheric CO_2 concentration, the subscript o represents the reference or background values, and the nonsubscripted concentration and isotopic ratio values represent the observations from any single, individual flask (Keeling et al. 2001).

We first establish this shift (Case 1) assuming, as in our double deconvolution calculations, that isotopic discrimination attending photosynthesis, α_{ab}, is constant. Then, for comparison (Case 2), we compute the shift if the proportions of photosynthesis owing to C_3 and C_4 plants vary, i.e., the forward and reverse fluxes, F_{ab} and F_{ba} of Equation 5.6 are equal. Finally, in Case 3, we compute the shift, if the properties of photosynthesis owing to C_3 and C_4 plants vary.

When we addressed concentration and isotopic ratio data that were obtained only after 1991, we found the latter more precise than obtained hitherto (Keeling et al. 2001). As expressed by Equations 5.6 to 5.9, the net flux, F_{bio}, and its ^{13}C equivalent, $*F_{bio}$, denote differences between much larger one-way fluxes, F_{ab}, F_{ba} and $*F_{ab}$, $*F_{ba}$, respectively. As previously noted, the respiratory flux, F_{ba}, is assumed to have no fractionation (α'_{ba} of Equation 5.8 of unity). Flux F_{ab}, which represents assimilation of CO_2 by plants through photosynthesis, exhibits fractionation, expressed by the factor, α'_{ab}.

We now consider the possibility that α'_{ab} varies temporally, whether directly, or by varying the proportions of F_{ab} contributed by C_3 and C_4 plants that have distinctly different degrees of carbon isotope discrimination. We disregard the small difference between α'_{ab} and α_{ab} (Heimann and Keeling 1989) and adopt the latter in subsequent expressions.

Substituting in Equation 5.7 the relations for $*F_{ab}$ and $*F_{ba}$, as given by Equations 5.11 and 5.12, we obtain for the net ^{13}C flux:

$$*F_{bio} = (r_b F_{ba} - \alpha_{ab} r_a F_{ab})(R_s/r_s) \tag{5.18}$$

To proceed we define a hypothetical chemical steady state for the terrestrial biosphere, in which assimilation and respiration balance globally for both ^{12}C

and ^{13}C. At this steady state F_{ba} equals F_{ab}, and F_{bio} and $*F_{bio}$ are both zero. Hence,

$$r_b = \alpha_{ab} r_a \tag{5.19}$$

and therefore the $^{13}C/^{12}C$ ratios of F_{ab} and F_{ba} are both equal to the $^{13}C/^{12}C$ ratio of the terrestrial biospheric carbon pool, r_b.

Let δ_a and δ_b denote, respectively, the reduced isotopic ratios, $\delta^{13}C$ of atmospheric CO_2 and carbon in the terrestrial biosphere. From the definition of $\delta^{13}C$,

$$r_i = (\delta_i + 1) r_s \tag{5.20}$$

where i stands for either a or b. Replacing r_a and r_b in Equation 5.19 according to Equation 5.20, replacing δ_{ab} by $\varepsilon_{ab} + 1$, according to Equation 5.16, and rearranging, the isotopic steady state condition, expressed in per mil notation, is such that

$$\delta_b - \delta_a = \varepsilon_{ab} \tag{5.21}$$

(disregarding a product of second order terms, $\varepsilon_{ab}\ \delta_a$).

For each of the three cases under consideration, let us assume that an initial steady state is displaced by an abrupt imbalance either in the one-way fluxes, F_{ab} and F_{ba}, which pertain to both isotopes, or only in the one-way ^{13}C fluxes, $*F_{ab}$ and $*F_{ba}$. In each case, for simplicity, we disregard a subsequent approach to a new steady state involving a change in δ_b of the terrestrial biospheric carbon pool. Thus, we compute the maximum possible shift in δ_a in response to a specified displacement from steady state.

Let N_{ao} denote the amount of CO_2 in the atmosphere, and δ_{ao} and δ_{bo} denote δ_a and δ_b, respectively, at the initial steady state. It follows from Equation 5.21 that the reduced isotopic ratios of both F_{ab} and F_{ba} are equal to δ_{bo}. We adopt 747.6 Pg C for N_{ao} based on a CO_2 concentration of 352.2 ppm for 1990, approximately the midpoint of our deconvolution calculations. In accord with our analysis of global average isotopic discrimination, $\varepsilon_{ab} = 15.32‰$.

Let ΔF_{bio} denote an abrupt departure of either of the one-way fluxes, F_{ba} or F_{ab}, or in both combined. Thus, in place of Equation 5.17

$$\Delta F_{bio} = F_{ba} - F_{ab} \tag{5.22}$$

Both F_{ba} and F_{ab}, as noted above, are assumed initially to have reduced isotopic ratios equal to δ_{bo}. In accord with Equation 5.17, and assuming that the departure from steady state has continued for a time-interval, ΔT, too short to cause significant changes in these isotopic ratios

$$N_{ao}\ \delta_{ao} + \Delta F_{bio} \Delta T\ \delta_{bo} = (N_{ao} + \Delta F_{bio} \Delta T)(\delta_{ao} + \Delta \delta_a) \tag{5.23}$$

where $\Delta\delta_a$ denotes the shift in the $^{13}C/^{12}C$ ratio of atmospheric CO_2 owing to the displacement from steady state. Solving for $\Delta\delta_a$ with δ_{bo}–δ_{ao} replaced by ε_{ab}, which is time-invariant according to Equation 5.21, and with $\Delta F_{bio}\Delta T << N_a$

$$\Delta\delta_a = \varepsilon_{ab}\Delta F_{bio}\Delta T/N_{ao} \tag{5.24}$$

$$= (-0.0205‰)\Delta F_{bio}\Delta T \tag{5.25}$$

Thus, a 1 Pg C yr^{-1} net flux of CO_2 from the biosphere to the atmosphere, acting for one year ($\Delta F_{bio}\Delta T = 1$), decreases the $\delta^{13}C$ value of atmospheric CO_2 by 0.0205‰; an opposite flux increases $\delta^{13}C$ by the same amount. (The product, $\varepsilon_{ab} \cdot \Delta F_{bio}$ represents an isotopic flux, 'isoflux,' between the terrestrial and atmospheric carbon pools, for this example equal to 15.32‰ Pg C yr^{-1}).

For Case 2, let $\Delta\varepsilon_{ab}$ denote a shift in discrimination for the full one-way flux, F_{ab}, with no change in $\delta^{13}C$ of the return flux, F_{ba}. Invoking Equation 5.17 as in Case 1, but with respect to both addition and subtraction of CO_2 by biospheric exchange:

$$N_{ao}\,\delta_{ao} + F_{ba}\Delta T\delta_{bo} - F_{ab}\Delta T\,(\delta_{bo} + \Delta\varepsilon_{ab}) = N_{ao}\,(\delta_{ao} + \Delta\delta_a) \tag{5.26}$$

Solving for $\Delta\delta_a$ with $F_{ab} = F_{ba}$,

$$\Delta\delta_a = -\Delta\varepsilon_{ab}\,F_{ab}\Delta T\,/N_{ao} \tag{5.27}$$

With F_{ab} set equal to our estimate of global NPP, 61.3 Pg C yr^{-1} and $\Delta\varepsilon_{ab}$ set, as an example, to 1‰, we obtain an isotopic shift, $\Delta\delta_a$, of 0.082‰ in one year, four times that evaluated in Case 1. The isoflux for this example, $\Delta\varepsilon_{ab} \cdot F_{ab}$, is 61.3‰ Pg C yr^{-1}. Even if the change in discrimination in Case 2 should occur only in the tropics, where our regional analysis indicates that most of the correlation of biospheric flux with El Niño events occurs, a 1‰ change in carbon isotope discrimination (with respect to an estimated tropical NPP of 32.8 Pg C yr^{-1}) would cause a shift of 0.044‰, more than twice that for a transfer of 1 Pg C of CO_2 in one year to or from the atmosphere according to Case 1.

For Case 3, a change occurs in the proportion of assimilation by C_4 plants, without a change in the fluxes with respect to C_3 and C_4 plants combined. The disequilibrium flux is equivalent to Case 1 except that it is applied separately for C_3 and C_4 plants with the added condition that the changes in net biospheric fluxes are equal and opposite for C_3 and C_4 plants. Denoting the mutual changes by ΔF_b, positive for increasing net C_3 flux to the atmosphere (cf. Equation 5.24)

$$\Delta\delta_a = ({}^3\varepsilon_{ab} - {}^4\varepsilon_{ab})\,\Delta F_b\,\Delta T/N_{ao} \tag{5.28}$$

$$= (-0.019‰)\,\Delta F_b\Delta T \tag{5.29}$$

where superscripts 3 and 4 distinguish the fractionation factors for C_3 and C_4 plants, respectively (17.8‰ and 3.6‰). A disequilibrium flux, ΔF_b, of 1 Pg C

yr^{-1} causes almost the same isotopic shift, $\Delta\delta_a$, as a 1 Pg C yr^{-1} change in NPP or respiration in Case 1, a result that could be anticipated because the substitution of a C_4 flux for a C_3 flux has almost the same effect on the $^{13}C/^{12}C$ of atmospheric CO_2 as a diminution in the overall net flux, F_{bio}.

Given the relatively small differences in isotopic discrimination by plants that may cause signals in the $^{13}C/^{12}C$ ratio of atmospheric CO_2 shown by these calculations, it may be unrealistic to assume in a double deconvolution that these signals are caused solely by variations in biospheric flux with isotopic discrimination fixed. Variations in carbon isotope discrimination of the order of 2‰ suggested by recent studies cited above, either from changes in discrimination or the fraction of NPP owing to C_4 plants, can produce signals that are comparable to those from varying net CO_2 exchange.

5.6 Global CO_2 Fluxes

Plots of the terms of the global atmospheric carbon cycle budget, expressed by Equation 5.3, are shown in Fig. 5.6 together with subordinate terms appearing in Equations 5.4 and 5.5. Fig. 5.6A shows the rate of industrial CO_2 emissions, F_{ind} (upper curve), and the rate of change in atmospheric concentration, dN_a/dt (middle curve)—terms that serve as inputs to the single deconvolution procedure. Their difference, $F_{bio} + F_{oce}$ (lower curve), constitutes a combined terrestrial biospheric and oceanic sink of industrial CO_2. In Fig 5.6B this sink is separated into biospheric and oceanic components, F_{bio} (thick curve), F_{oce} (thin curve), respectively, as determined by the double deconvolution procedure. In Panel C the biospheric component is shown divided into three fluxes: F_{fer}, a "CO_2 fertilization sink," representing the response of the terrestrial biosphere to increasing atmospheric CO_2 concentration, an assumed constant "land-use source," F_{des}, of 2.0 PgC yr^{-1} representing human-induced release of terrestrial CO_2, and an "anomalous biospheric flux," $F_{ano,bio}$, that is presumed to result mainly from natural variability in the carbon cycle, although it may also reflect variability in human disturbances not accounted for by F_{fer} and F_{des}. Also shown (dashed curve) is a revision of the anomalous biospheric oceanic flux in which isotopic variations are ignored, equivalent to assuming that they principally reflect changes in discrimination by plants. In Panel D the oceanic component is shown divided into an oceanic "uptake sink," a response to increasing atmospheric CO_2, F_{ex}, and an "anomalous oceanic flux," $F_{ano,oce}$, mainly, or entirely, of natural origin. If isotopic variations are ignored, as in the dashed curve in Fig 5.6C, the uptake sink remains as shown, but the anomalous oceanic flux is reduced to zero for all times.

We first address the average strengths of these terms of the carbon cycle budget equation. As shown in Table 5.1, averages of the terms plotted in Fig. 5.6 for the 1980s agree within 0.2 Pg C yr^{-1} with corresponding fluxes reported by Houghton et al. in the Intergovernmental Panel on Climate Change, Second Assessment Report to the United Nations (IPCC, 1996), altered only slightly in a Third Assessment Report (IPCC, 2001). Agreement is also close for the 1990s

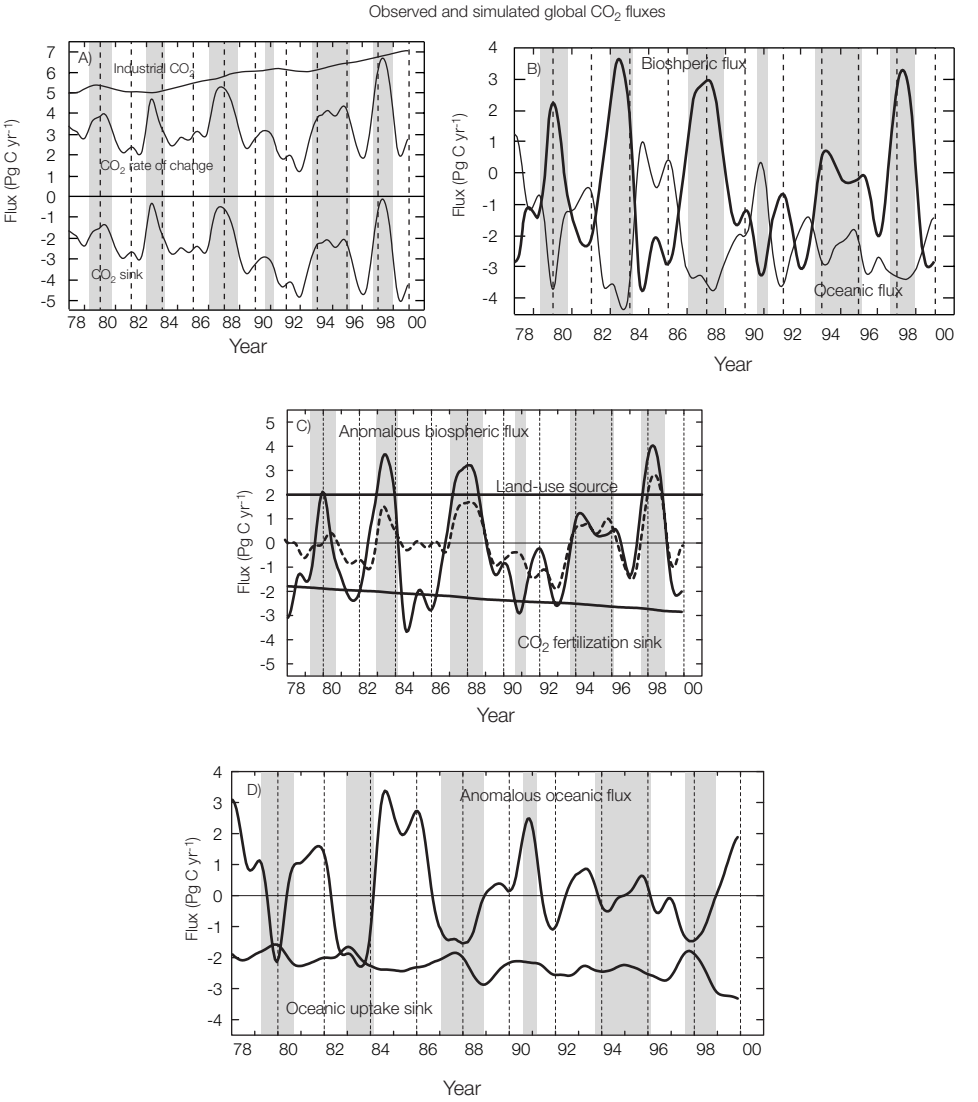

Figure 5.6. Time varying global CO_2 fluxes, in Pg C yr^{-1}, as labeled, positive to the atmosphere, shown as spline fits to monthly data. Gray bars are as in Fig. 5.4. **(A)** Industrial CO_2 emissions, rate of change of CO_2 abundance, and an inferred atmospheric CO_2 sink, defined as the difference between emissions and abundance change. **(B)** Net terrestrial biospheric and oceanic CO_2 exchange fluxes with the atmosphere (thick and thin lines, respectively), computed by double deconvolution as described in the text, assuming constant isotopic discrimination for C_3 and C_4 plants. **(C)** The terrestrial biospheric exchange flux, shown in Panel B, divided into a contribution related to rising atmospheric CO_2 concentration, F_{fer} ("CO_2 fertilization flux," lower curve), a constant "land-use source", F_{des} (straight line), and an anomalous flux, $F_{ano,bio}$, as defined in the text. Also shown (dashed curve) is an alternative estimate of the anomalous biospheric flux in which isotopic variations are ignored. **(D)** Oceanic exchange flux of Panel B, divided into an oceanic uptake flux (F_{ex}, lower curve) and an anomalous flux, $F_{ano,oce}$, as defined in the text.

Table 5.1. Global Net Carbon Dioxide Fluxes, in PgC yr^{-1}, obtained by double deconvolution compared with fluxes of IPCC Reports. Fluxes are positive into the atmosphere. Fluxes reported by IPCC (1996, 2001) have errors quoted here at 90% confidence ($\pm 2\sigma$). Those for 1990 to 1999 are doubled from 67% confidence levels quoted by IPCC (2001).

	1980–1989		1990–1999	
Period covered:	IPCC	Present Analysis	IPCC	Present Analysis
Atmosphere increase:	$+3.3 \pm 0.2$	$+3.3$	3.2 ± 0.2	$+3.3$
Emissions from fossil fuel combustion and cement production:	$+5.5 \pm 0.5$	$+5.44$	6.4 ± 0.8	$+6.41$
Net oceanic uptake:	-2.0 ± 0.8	-2.0	-1.7 ± 0.5	-2.4
Net emissions from changes in tropical land-use:	$+1.6 \pm 1.0$		insufficient data	
Uptake by Northern Hemisphere forest regrowth:	-0.5 ± 0.5		insufficient data	
Other terrestrial sinks:	-1.3 ± 1.5		insufficient data	
Combined terrestrial biospheric flux:	-0.2 ± 1.9	-0.2	-1.4 ± 1.4	-0.8

with respect to atmospheric CO_2 increase and emissions of fossil fuel CO_2, but we find a substantially larger oceanic uptake of atmospheric CO_2 (by 0.7 Pg C yr^{-1}) than the IPCC and a smaller biospheric uptake (by 0.6 Pg C yr^{-1}). These disagreements are within the range of uncertainty in the absolute magnitude of the IPCC budget estimates when expressed at 90% confidence, but this range is so large that the relative importance of the oceans and terrestrial biosphere in removing industrial CO_2 from the air evidently cannot yet be determined reliably.

The flux estimates just described also reveal variability in the atmospheric CO_2 budget on the decadal time-scale. In agreement with the IPCC we find that atmospheric CO_2 rose at nearly the same rate in the 1980s and 1990s in spite of an increase in CO_2 emissions from fossil fuel combustion of 0.9 Pg C yr^{-1}. These changes are well established, because uncertainty in absolute magnitudes as stated by the IPCC reflect, to a considerable degree, biases that don't change appreciably from one decade to the next.

Estimates of decadal changes in the oceanic and terrestrial biospheric CO_2 exchange fluxes are less certain. We find an increased oceanic sink by relying on a double deconvolution calculation that takes account of changing $\delta^{13}C$, based on data acquired using consistent procedures of both sampling and measurement. The calculations are sensitive to model assumptions regarding how global terrestrial biospheric and oceanic reservoirs respond to perturbations induced by changing atmospheric CO_2. The IPCC in their Third Assessment Report found a reduced oceanic sink by interpreting a shift in the O_2/N_2 ratio in the atmosphere as measured in the 1980s from archived air samples compared to direct mea-

surements in the 1990s. The change in data source from decade to decade contributes uncertainty to some unknown degree, and the results are subject to modeling uncertainty not yet fully established, because of aspects of the oceanic carbon cycle, such as outgassing of oxygen, that are not fully understood. Thus, it is not possible with any great confidence to decide whether a diminishing oceanic sink and an increasing terrestrial biospheric sink, as reported by the IPCC, are more likely to be correct than our finding of increases in both sinks. An important finding on which we agree with the IPCC qualitatively is that the terrestrial biospheric exchange flux increased from the 1980s to the 1990s.

Interannual variations in the fluxes of the budget Equation 5.3 over a shorter term, summarized by the IPCC (2001), are also of interest. Such variations in the rate of change in atmospheric CO_2 concentration, dN_a/dt, and in industrial CO_2 emissions, F_{ind}, shown by the two upper curves of Fig. 5.6A, are both well determined, the former derived from our atmospheric observations, the latter from Andres et al. (2000), the same international statistical data used by IPCC. Variations in their difference, equal to $F_{oce} + F_{bio}$, are therefore also well determined. This combined oceanic and terrestrial sink (lower curve in Fig. 5.6A), indeed, has nearly the same interannual pattern of variability as the change in atmospheric CO_2 concentration, dN_a/dt, because global industrial CO_2 emissions, F_{ind}, vary only slightly from year to year. Most notable are maxima in $F_{oce} + F_{bio}$ close to time-intervals shown by vertical gray bars, suggesting a coupling of both oceanic and terrestrial carbon cycle components with globally average warm periods, often El Niño events, as discussed earlier.

The oscillatory pattern of variations in F_{bio} (Panel B), especially its phasing, is so similar to that of dN_a/dt and $F_{oce} + F_{bio}$ (Panel A) that F_{bio} appears to represent the predominant cause of short-term interannual variability in dN_a/dt. The calculated amplitudes of the prominent fluctuations in F_{bio}, however, substantially exceed those in dN_a/dt, resulting in opposing patterns in the oceanic and biospheric fluxes, as discussed below.

In summary, the decadal averages of F_{bio} and F_{oce}, as listed in Table 5.1, are dependent on the choice of oceanic submodel used in the deconvolution procedure. The short-term interannual variability in the anomalous fluxes, $F_{ano,bio}$ and $F_{ano,oce}$, however, is closely prescribed by the CO_2 observations, provided that isotopic discrimination is correctly specified, as discussed below.

5.7 Reliability of Deduced Fluxes

Before discussing our findings regarding the global average terrestrial and oceanic fluxes, F_{bio} and F_{oce}, we will examine the extent of possible errors in the calculations. We address uncertainty in our results on several time-scales.

Statistical errors in F_{bio} and F_{oce}, on short time-scales, are contributed by scatter in the data for both concentration and $^{13}C/^{12}C$ ratio, expressed by standard

errors of the fit of individual observations to the spline curves shown in Fig. 5.3. These errors range from 0.15 ppm and 0.02‰ at the South Pole to 1.1 ppm and 0.07‰ at Point Barrow, Alaska, and result in errors of the order of 0.5 Pg C yr^{-1} with respect to F_{bio} and F_{oce}, as discussed by Piper et al. (2001). Thus, although significant, these errors are not large enough to challenge our finding of large short-term interannual fluctuations in biospheric and oceanic fluxes (of the order of several Pg C yr^{-1}). A more important issue is whether the calculation of these fluxes is affected by systematic errors, which is possible on all time-scales.

We first discuss possible errors associated with the double deconvolution procedure, which deduces fluxes from simultaneous data for the concentration and $^{13}C/^{12}C$ ratio of atmospheric CO_2. We thus add to our earlier discussion of uncertainties on the decadal time-scale. We then discuss errors on the short-term interannual time-scale, approximately that of the ENSO cycle.

To deduce the relative strengths of F_{bio} and F_{oce}, which include responses to the combustion of fossil fuels, we have made use of the same inverse double deconvolution procedure used previously by Keeling et al. (1989a, 1995). Previously, however, only anomalous fluxes were calculated, similar to $F_{ano,bio}$ and $F_{ano,oce}$, plotted in Fig. 5.6C,D. Here, full net fluxes, denoted by F_{bio} and F_{oce}, are also calculated, as plotted in Fig. 5.6B. As pointed out above, the validity of the deduced average magnitude of these fluxes depends on the correctness of the oceanic submodel used in the deconvolution procedure.

Although our study addresses interannual variability of the global carbon cycle over two decades, it does not resolve decadal variability and the so-called missing CO_2 sink issue (Wigley and Schimel 2000) regarding whether the terrestrial biosphere is an important global sink for CO_2 produced by the combustion of fossil fuels as discussed above.

The principal components of the global atmospheric CO_2 budget are known with widely varying uncertainties. As estimated by the IPCC (Table 5.1) at 90% confidence, the independent errors associated with the rate of increase of atmospheric CO_2 (± 0.20 Pg C yr^{-1}) and industrial CO_2 emissions (± 0.50 Pg C yr^{-1}) are so small that the error in the combined oceanic-terrestrial biospheric flux, $F_{oce} + F_{bio}$, is uncertain to only ± 0.54 Pg C yr^{-1} (calculated by quadrature). The errors for the separate oceanic and terrestrial biospheric fluxes alone are substantially larger. When determined from separate errors for three components, the error for F_{bio} is ± 1.9 Pg C yr^{-1}. Such a large error is not surprising since data must be assembled globally for many diverse pools of carbon. A substantially lower error for F_{bio}, ± 0.9 Pg C yr^{-1}, is obtained when determined by subtracting estimates of F_{oce} from the sum $F_{oce} + F_{bio}$, the approach of the IPCC, underscoring the value in obtaining precise estimates of oceanic uptake of atmospheric CO_2 as an indirect approach to determining the global average of the terrestrial biospheric flux F_{bio}, as discussed further below.

Both the terrestrial and oceanic CO_2 fluxes inferred from our atmospheric CO_2 data show a distinct association with fluctuating temperature, most evident

during El Niño events when the concentration of atmospheric CO_2 has risen most rapidly. This association with the ENSO cycle is not surprising because these events are attended by pronounced changes in the temperature and circulation of both the atmosphere and the oceans that are likely to affect the global terrestrial and oceanic carbon pools. Thus the phasing of the large fluctuations seen in our atmospheric data are not difficult to explain, but our finding of large opposing terrestrial releases and oceanic sinks of CO_2 phased with the ENSO cycle has been challenged on the grounds that our $^{13}C/^{12}C$ data through 1988 (Keeling et al. 1989a) contain substantial systematic errors, specifically that they do not agree with other measurements showing only small isotopic fluctuations with little association with the strong El Niño events in 1982–3 and 1987–8 (Francey et al. 1995).

Although two succeeding El Niño events, in 1992 and 1994, were not strong enough to substantiate the plausibility of the large fluctuations that our data show for the 1980s, we now possess data for an El Niño event in 1997–98, for which the rate of change in $^{13}C/^{12}C$ ratio (see Fig. 5.5) fluctuated with an amplitude as large as that found for the strong events in 1982–83 and 1987–88. Furthermore, this fluctuation, as were fluctuations for the El Niño events of 1982–83 and 1987–88, is seen separately for every station in our array.

Although calibrating errors cannot be ruled out, a more likely source of systematic error is some shortcoming in either the terrestrial biospheric or oceanic submodel of the double deconvolution procedure. A likely possibility is our assumption that isotopic discrimination attending photosynthesis on land is constant. If we assume that isotopic variability is caused solely by variable isotopic discrimination by plants, fluctuations in the biospheric flux for the strong events of 1982–83, 1987–88, and 1997–98 are reduced by nearly two-thirds, as shown by comparing the solid and dashed anomalous biospheric flux curves of Fig. 5.6B. For these events, fluctuations in the oceanic flux are not just reduced but are reversed in phase to the pattern shown by the oceanic uptake flux in Fig. 5.6C. Even if variability in discrimination is only 1 ‰, fluctuations in the biospheric flux are substantially reduced and the opposing oceanic fluxes eliminated. Tropical drought and heat attending El Niño events are expected to cause stress in plants so that net primary production (NPP) decreases and atmospheric CO_2 rises anomalously, as observed. Perhaps a decrease in discrimination accompanies this presumed decrease in NPP, such that the two effects cannot be distinguished because their timing is too similar.

Evidence, reported by Piper et al. (2001), shows that the association of terrestrial biospheric and oceanic CO_2 fluxes with warming events occurs mostly in the tropics. Correlations of these inferred fluctuations with variations in climatic factors therefore should reflect a relation of climate forcing to the metabolic activity of plants in which the phasing is well determined even if the magnitudes of the fluctuations are poorly established from the atmospheric data. We thus may gain insight into the relationship of the carbon cycle to climate without yet knowing the extent of variable discrimination by tropical plants.

5.8 Short-Term Variability in the Global Carbon Cycle

To compare the magnitude of fluctuations in exchange fluxes with the strength of El Niño events, we again turn to the southern oscillation index (SOI), which tracks the ENSO cycle. For the period of our study, from 1978 to 1999, the most pronounced fluctuations in SOI occurred near the times of strong El Niño events of 1982–83, 1987–88, and 1997–98 (henceforth, events of 1983, 1987, and 1998). We ask, to what degree did extremes seen in the anomalous biospheric and oceanic fluxes, $F_{ano,bio}$ and $F_{ano,oce}$ represent responses to climatic variability at these times?

Because the amplitudes of the fluctuations in SOI are nearly equal for these three El Niño events, it is possible that they reflect approximately equal climatic forcing. Calculated amplitudes of fluctuations in the anomalous biospheric flux, $F_{ano,bio}$ (see Fig. 5.6C, solid curve) for these events are also nearly equal, based on our observing nearly equal amplitudes of corresponding fluctuations in rate of change of $^{13}C/^{12}C$ ratio (see Fig. 5.5). The calculated fluctuation in the anomalous oceanic flux, $F_{ano,oce}$ (see Fig. 5.6D), however, is of lesser amplitude for the 1998 event than for either of the two previous events, reflecting a greater fluctuation in the rate of change of atmospheric CO_2 for this event (see Fig. 5.5). How can this lesser oceanic fluctuation be explained?

Either the fluctuations in the oceanic flux, indeed, were different in spite of similar signals in the SOI for all three events, or the terrestrial biospheric flux has been incorrectly calculated. We first discuss the likelihood of variable oceanic fluctuations. In a previous double deconvolution calculation with data only through 1988 (Keeling et al. 1989a), variations in $F_{ano,oce}$ showed a correlation with tropical sea surface temperature. In the updated analysis, east tropical Pacific sea surface temperature showed greater warming for the 1998 El Niño event than for the events of 1983 and 1987, whereas the oceanic sink was less pronounced. Thus variable fluctuations in tropical sea surface temperature do not explain quantitatively a smaller oceanic fluctuation in 1998.

Alternatively, neglecting to account for temporal variability in isotopic discrimination by plants may have caused errors in the calculated fluxes. Although the nearly equal amplitudes of fluctuations in the first derivative of $\delta^{13}C$ of atmospheric CO_2 that we observe in association with El Niño events (see Fig. 5.5) suggest corresponding nearly equal amplitudes in $F_{ano,bio}$, perhaps this is not a correct conclusion. This flux reflects both anomalous assimilation of carbon by net primary production (NPP) and anomalous release of biospheric carbon by respiration. Although respiration, as well as NPP, generally responds directly to variability in temperature and precipitation, the sensitivities are not necessarily the same. Variations in NPP, respiration, and variable isotopic discrimination could fortuitously lead to our calculating nearly the same amplitudes for fluctuations associated with the three strong El Niño events of 1983, 1987, and 1998 by ignoring variations in discrimination.

5.9 Ways to Reduce Uncertainty in Estimation of Exchange Fluxes

Given the present difficulties in inferring CO_2 fluxes from atmospheric CO_2 data as discussed above, several possible improvements come to mind. One that is obvious is to increase the precision and absolute accuracy of time-series data. Better calibrations would almost surely improve the database for studying fluxes, especially with respect to isotopic data. In particular they would prevent the finding of such large differences in results between laboratories that one laboratory may find a large isotopic El Niño signal while another does not. Most helpful would be the reintroduction of international isotopic standard reference materials, in the range of oceanic and atmospheric CO_2, for systematic long-term intercalibration between laboratories.

Uncertainty in establishing the rate of uptake of atmospheric CO_2 by the oceans presently limits our ability to identify which part of the combined oceanic and terrestrial sink of industrial CO_2 is oceanic, because the terrestrial biospheric sink is, and probably will remain, far less well determined than the oceanic sink. Several indirect means to improve knowledge of the oceanic sink have been pursued: studies of the fundamental behavior of the oceanic carbon cycle through oceanic campaigns, such as the JGOFS program; investigations of the ocean circulation, such as was pursued by the World Ocean Circulation Experiment; and the use of transient tracers, such as chlorofluorocarbons to define better in general the transport of chemical substances in the oceans. The present uncertainty in the oceanic sink (see Table 5.1) takes into account all of these techniques.

Given the dependency of the double deconvolution procedure on the choice of oceanic submodel, as discussed above, there is no means of estimating the correctness of the average magnitudes of net oceanic fluxes from atmospheric CO_2 data alone. The determination of F_{oce} would be better determined if time-series were available adequate to establish the global average of $^{13}C/^{12}C$ ratio of dissolved inorganic carbon (DIC) in surface ocean water, and still better if adequate subsurface isotopic data were also available (Quay, Tilbrook, and Wong 1992). However, no indirect method is likely to be as reliable as direct measurements of DIC, such as were pursued during the World Oceans Circulation Experiment (Needler 1992). Such measurements, however, should be carried out repeatedly to establish the rate of change of the inventory of carbon in the world oceans.

Independently establishing the global exchange of atmospheric CO_2 with the terrestrial biosphere, either by direct flux measurements or by measuring the changing inventory of carbon in plants and sinks, is not likely to produce a precise global inventory for terrestrial biospheric carbon because of the great heterogeneity of the reservoir. Thus the extent to which the terrestrial biosphere is a source or sink of atmospheric CO_2 globally will probably be best determined by subtracting from the well-established combined sink, $F_{bio} + F_{oce}$, the estimates of the oceanic flux, F_{oce}, based on direct oceanic inventory data. This approach has long-term merit because the data gain more and more significance as the time-interval of measurements lengthens.

A third approach is to use precise measurements of atmospheric oxygen concentration concurrently with measurements of CO_2 concentration and $^{13}C/^{12}C$ ratio, further to constrain the relative magnitudes of the oceanic and terrestrial CO_2 exchange fluxes. Atmospheric oxygen is influenced by exchanges with the land and oceans in different proportions than is carbon dioxide, so the combination of atmospheric O_2 and CO_2 measurements can help to resolve the relative proportions of the land and ocean carbon sinks (Keeling and Shertz 1992; Battle et al. 2000). This method, as all other known methods, has complications but is likely to produce valuable evidence of the time-evolution of oceanic uptake on all time-scales from seasonal to long term, complementing direct measurements of increasing carbon in seawater that can be made worldwide only at infrequent intervals.

5.10 Summary

Combined measurements of the concentration and $^{13}C/^{12}C$ isotopic ratio of atmospheric CO_2 have provided us with a basis for distinguishing terrestrial biospheric and oceanic exchanges of CO_2, from 1978 through 1999. We find remarkably similar patterns of fluctuations of variations in concentration and isotopic ratio on the time-scale of the El Niño–southern oscillation (ENSO) cycle, from which we infer increased releases of CO_2 by the terrestrial biosphere, partially offset by greater uptake of CO_2 by the oceans during El Niño events and at other times of above-average global temperature. Not all details of these correlations, however, are readily explained.

The best-established correlation of our atmospheric CO_2 data with the ENSO cycle pertains to the sum of the global biospheric and oceanic fluxes, established unambiguously by the rate of change in CO_2 concentration. The global average rate of change in $^{13}C/^{12}C$ ratio, though less well established, varies closely in phase with the global CO_2 concentration. It follows, therefore, that the global terrestrial biospheric flux, which the isotopic record reflects, almost certainly has correlated with the ENSO cycle. The global oceanic flux probably also correlates because it is determined by subtracting the biospheric flux from the sum of the two fluxes.

The amplitudes of fluctuations in this sum, derived solely from CO_2 concentration data, are also well established, but the amplitudes relating to the separate global biospheric and oceanic fluxes are uncertain. First, miscalibration of the isotopic data, and an inability to interpret these data correctly, may have produced errors in calculating amplitudes. Second, our isotopic data may reflect phenomena, particularly interannual variability in isotopic discrimination by plants, not considered in our calculations of fluxes. The similarity in phasing of variations in concentration and isotopic ratio demands, however, that possible variations in isotopic discrimination by plants, or other neglected phenomena, be phased consistently with fluctuations in the global biospheric flux.

It is, indeed, possible that phasing of variable discrimination is closely tied

to the ENSO cycle. The regional analysis of Piper et al. (2001) demonstrates that most of the correlation of biospheric flux with the ENSO cycle occurs in the tropics, where drought may cause both the net primary production of plants and the discrimination to decrease during El Niño events. Also, as discussed above, the existence of small average variations in tropical discrimination may explain a substantial part of the amplitude in biospheric fluctuations that we infer. However, the anticorrelation of oceanic flux with tropical sea surface temperature that we deduce supports the hypothesis that discrimination by plants may have varied only slightly over the ENSO cycle, or not at all. Such an anticorrelation is consistent with observed decreases in upwelling of cold CO_2-laden subsurface water in the tropics during El Niño events, expected to produce increased sea surface temperature together with a release of CO_2 to the air.

Quantitatively it is difficult to decide which mechanism best explains the observed amplitudes of major short-term interannual fluctuations in CO_2 concentration and $^{13}C/^{12}C$ ratio. The southern oscillation index (SOI), a measure of the intensity of El Niño events, shifts by nearly the same amount during three major events in 1983, 1987, and 1998 (the timing of which shows a close relation to the gray bars in Fig. 5.4). Tropical sea surface temperature also shows nearly equal shifts for these events. Nevertheless, the oceanic flux that we infer shows a substantially lesser fluctuation in 1998 than during the two earlier events, a finding not readily explained. Fluctuations in the rate of change of $^{13}C/^{12}C$ ratio for these three events are nearly the same, consistent with nearly equal strengths of the El Niño events as indicated by the SOI and sea surface temperature data. A reduction in amplitude owing to reduced discrimination is therefore expected to diminish, by similar amounts, the biospheric signals for all three events. Thus, if our isotopic data are correct, at least one signal, either oceanic or biospheric, must vary in strength between the events of the 1980s and the 1998 event. At present we cannot reconcile these uncertainties in interpretation.

Because so much of the interannual variability in CO_2 exchange deduced in our study is short term and attributed to a naturally occurring ENSO cycle, we have not dwelt at length on long-term variability in exchange or on anthropogenic factors that cause variability. The double deconvolution procedure that we have used takes account of the unquestionably human-caused rise in atmospheric CO_2 resulting from the combustion of fossil fuel, but this combustion process is sufficiently steady over the short term that it contributes but little to the interannual variability in atmospheric CO_2 on the ENSO timescale. Short-term variability is likely, however, to be partly of human cause, because of recent changes in land-use that may have increased the sensitivity of the terrestrial biosphere to natural variations in climatic factors: for example, indirectly by human-caused changes in albedo and latent heat exchange, or directly by causing more and greater forest and grass fires during periods of drought.

Our principal finding from this analysis of atmospheric CO_2 data is that interannual fluctuations in net exchanges of atmospheric CO_2 are of the order of

several Pg C yr^{-1} and correlate with strong El Niño events. The fluctuations clearly involve the terrestrial biosphere and probably the oceans, but their separate amplitudes and phasing cannot yet be precisely determined.

References

Andres, R.J., G. Marland, T. Boden, and S. Bischof. 2000. Carbon dioxide emissions from fossil fuel consumption and cement manufacture, 1751–1991 and an estimate of their isotopic composition and latitudinal distribution. In *The carbon cycle*, ed. T.M.L. Wigley and D.S. Schimel, 53–62. Cambridge: Cambridge University Press.

Andronova, N.G., and M.E. Schlesinger. 2000. Causes of global temperature changes during the 19th and 20th centuries. *Geophysical Research Letters* 27:2137–40.

Aubinet, M., A. Grelle, A. Ibrom, C. Rannik, J. Moncrieff, T. Foken, A.S. Kowalski, P.H. Martin, P. Berbigier, C. Bernhofer, R. Clement, J. Elbers, A. Granier, T. Grunwald, K. Morgenstern, K. Pilegaard, C. Rebmann, W. Snijders, R. Valentini, T. Vesala. 2000. Estimates of the annual net carbon and water exchange of forests: The EUROFLUX methodology. *Advances in Ecological Research* 30:113–75.

Bacastow, R.B. 1976. Modulation of atmospheric carbon dioxide by the southern oscillation. *Nature* 261:116–18.

Battle, M., M.L. Bender, P.P. Tans, J.W.C. White, J.T. Ellis, T. Conway, and R.J. Rancey. 2000. Global carbon sinks and their variability inferred from atmospheric O_2 and $\delta^{13}C$. *Science* 287:2467–70.

Canadell, J., H.A. Mooney, D. Baldocchi, J.A. Berry, J.R. Ehleringer, C.B. Field, S.T. Gower, D. Hollinger, J. Hunt, R. Jackson, S. Running, G. Shaver, S.E. Trumbore, R. Valentini, and B.Y. Bond. 2000. Carbon metabolism of the terrestrial biosphere: a multi-technique approach for improved understanding. *Ecosystems* 3:115–30.

Climate Prediction Center. [date] Monthly Atmospheric and SST Indices. Website: *www.cpc.ncep.noaa.gov/data/indices*.

Craig, H. 1957. Isotopic standards for carbon and oxygen and correction factors for mass-spectrometric analysis of carbon dioxide. *Geochimica et Cosmochimica Acta* 12:133–49.

Crowley, P.J. 2000. Causes of climate change over the past 1000 years. *Science* 289:270–77.

Ehleringer, J.R., A.E. Hall, and G.D. Farquhar, eds. 1993. Stable isotopes and plant carbon/water relations. San Diego: Academic Press.

Etheridge, D.M., L.P. Steele, R.L. Langenfelds, R.J. Francey, J.M. Barnola, and V.I. Morgan. 1996. Natural and anthropogenic changes in atmospheric CO_2 over the last 1000 years from air in Antarctic ice and firn. *Journal Geophys. Research—Atmospheres* 101(D2):4115–28.

Falkowski, P., R.J. Scholes, E. Boyle, J. Canadell, D. Canfield, J. Elser, N. Gruber, K. Hibbard, P. Hogberg, S. Linder, F.T. Mackenzie, B. Moore, T. Pedersen, Y. Rosenthal, S. Seitzinger, V. Smetacek, and W. Steffen. 2000. The global carbon cycle: A test of our knowledge of earth as a system. *Science* 290:291–96.

Farquhar, G.D., J.R. Ehleringer, and K.T. Hubick. 1989. Carbon isotope discrimination and photosynthesis. *Annual Review Plant Physiology and Molecular Biology* 40:503–37.

Fessenden, J.E., and J.R. Ehleringer. 2003. Temporal variation in $\delta^{13}C$ of ecosystem respiration in the Pacific Northwest: Links to moisture stress. *Oecologia* 136:129–36.

Francey, R.J., P.P. Tans, C.E. Allison, I.G. Enting, J.W.C. White, and M. Trolier. 1995. Changes in oceanic and terrestrial carbon uptake since 1982. *Nature* 373:326–30.

Free, M., and A. Robock. 1999. Global warming in the context of the Little Ice Age. *Journal of Geophysical Research* 104:19,057–19,070.

Heimann, M., and C.D. Keeling. 1989. A three-dimensional model of atmospheric CO_2 transport based on observed winds: 2. Model description and simulated tracer experiments. In *Aspects of climate variability in the Pacific and Western Americas*, Geophysical Monograph 55, ed. D.H. Peterson, 237–75. Washington D.C.: American Geophysical Union.

Heimann, M., C.D. Keeling, and C.J. Tucker. 1989. A three-dimensional model of atmospheric CO_2 transport based on observed winds: 3. Seasonal cycle and synoptic time scale variations. In *Aspects of climate variability in the Pacific and the Western Americas,* Geophysical Monograph 55, ed. D.H. Peterson, 277–303. Washington, D.C.: American Geophysical Union.

Houghton, J.T., Y. Ding, D.J. Griggs, M. Noguer, P.J. van der Linden, X. Dai, K. Maskell, and C.A. Johnson. 2001. Climate change 2001, the scientific basis. Contribution of Working Group I to the Third Assessment Report of the Intergovernmental Panel on Climate Change (IPCC). Cambridge: Cambridge University Press.

Houghton, J.T., L.G. Meira Filho, B.A. Callander, N. Harris, A. Kattenberg, and K. Maskell. 1996. Climate change 1995, the science of climate change. Contribution of Working Group I to the Second Assessment Report of the Intergovernmental Panel on Climate Change (IPCC). Cambridge: Cambridge University Press.

Houghton, R.A. 1999. The annual net flux of carbon to the atmosphere from changes in land use 1850–1990. *Tellus* 51B:298–313.

Hunt, E.R., S.C. Piper, R. Nemani, C.D. Keeling, R.D. Otto, and S.W. Running. 1996. Global net carbon exchange and intra-annual atmospheric CO_2 concentrations predicted by an ecosystem process model and three-dimensional atmospheric transport model. *Global Biogeochemical Cycles* 10:431–56.

Jones, P.D. 1994. Hemispheric surface air temperature variations: a reanalysis and an update to 1993. *Journal of Climate* 7:1794–1802.

Karl, D.M., and A.F. Michaels. 1996. Tropical studies in oceanography. *Deep-Sea Research* 43:127–28.

Keeling, C.D., R.B. Bacastow, A.F. Carter, S.C. Piper, T.P. Whorf, M. Heimann, W.G. Mook, and H. Roeloffzen. 1989a. A three-dimensional model of atmospheric CO_2 transport based on observed winds: 1. Analysis of observational data. In *Aspects of climate variability in the Pacific and the Western Americas,* Geophysical Monograph, 55, ed. D.H. Peterson, 165–236. Washington, D.C.: American Geophysical Union.

Keeling C.D., S.C. Piper, R.B. Bacastor, M. Wahlen, T.P. Whorf, M. Heimann, and H.A. Meijer. 2001. Exchanges of atmospheric CO_2 and $^{13}CO_2$ with the terrestrial biosphere and oceans from 1978 to 2000. I. Global aspects. *SIO Reference Series,* No. 01–06. San Diego: Scripps Institution of Oceanography.

Keeling, C.D., S.C. Piper, and M. Heimann. 1989b. A three-dimensional model of atmospheric CO_2 transport based on observed winds: 4. Mean annual gradients and interannual variations. In *Aspects of climate variability in the Pacific and the Western Americas,* Geophysical Monograph, 55, ed. D.H. Peterson, 305–63. Washington, D.C.: American Geophysical Union.

Keeling, C.D., T.P. Whorf, M. Wahlen, and J. Van der Plicht. 1995. Interannual extremes in the rate of rise of atmospheric carbon dioxide since 1980. *Nature* 375:666–70.

Keeling, R.F., and S.R Shertz. 1992. Seasonal and interannual variations in atmospheric oxygen and implications for the global carbon cycle. *Nature* 358:723–27.

Lloyd, J., and G.D. Farquhar. 1994. C-13 discrimination during CO_2 assimilation by the terrestrial biosphere. *Oecologia* 99:201–15.

Meehl, G.A. 1987. The annual cycle and interannual variability in the tropical Pacific and Indian ocean regions. *Monthly Weather Review* 115:27–50.

Mook, W.G., and P.M. Grootes. 1973. The measuring procedure and corrections for the high-precision mass-spectrometric analysis of isotopic abundance ratios, especially referring to carbon, oxygen and nitrogen. *International Journal of Mass Spectrometry and Ion Physics* 12:273–98.

Mook, W.G., M. Koopmans, A.F. Carter, and C.D. Keeling. 1983. Seasonal, latitudinal and secular variations in the abundance and isotopic ratios of atmospheric carbon dioxide: 1. Results from land stations. *Journal of Geophysical Research* 88:10915–33.

Needler, G.T. 1992. The World Ocean Circulation Experiment. *Oceanus* 35:74–77.

Ometto, J.P.H.B., L.B. Flanagan, L.A. Martinelli, M.Z. Moreira, N. Higuchi, and J.R. Ehleringer. 2002. Carbon isotope discrimination in forest and pasture ecosystems of the Amazon Basin, Brazil. *Global Biogechemical Cycles* 16 (December):article 1109.

Pataki, D.E., J.R. Ehleringer, L.B. Flanagan, D. Yakir, D.R. Bowling, C.J. Still, N. Buchmann, J.O. Kaplan, and J.A. Berry. 2003. The application and interpretation of Keeling plots in terrestrial carbon cycle research. *Global Biogeochemical Cycles* 17 (March):article 1022.

Piper, S.C., C.D. Keeling, M. Heimann, and E.F. Stewart. 2001. Exchanges of atmospheric CO_2 and $^{13}CO_2$ with the terrestrial biosphere and oceans from 1978 to 2000. II. A three-dimensional tracer inversion model to deduce regional fluxes. In *SIO Reference Series,* no. 01–07. San Diego: Scripps Institution of Oceanography.

Quay, P.S., B. Tilbrook, C.S. Wong. 1992. Oceanic uptake of fossil fuel CO_2: Carbon-13 evidence. *Science* 256:74–79.

Rasmusson, E.M., and J.M. Wallace. 1983. Meteorological aspects of the El Niño/southern oscillation. *Science* 222:1195–1202.

Santer, B.D. et al. 1996. Detection of climate change and attribution of causes. In *Climate Change 1995,* ed. J.T. Houghton et al., 407–11. Cambridge: Cambridge University Press.

Siegenthaler, U., and H. Oeschger, H. 1987. Biospheric CO_2 sources emissions during the past 200 years reconstructed by deconvolution of ice core data. *Tellus* 39B:140–54.

Slingo, J.M., and H. Annamalai. 2000. 1997: The El Niño of the century and the response of the Indian summer monsoon. *Monthly Weather Review* 12:1178–97.

Still, C.J., J.A. Berry, G.J. Collatz, and R.S. DeFries. 2003. Global distribution of C_3 and C_4 vegetation: Carbon cycle implications. *Global Biogeochemical Cycles* 17 (January):article 1006.

Wigley, T.M.L., and D.S. Schimel. 2000. *The carbon cycle.* New York: Cambridge University Press.